Inorganic Chemistry

Article

pubs.acs.org/IC

Efficient Near-Infrared Downconversion and Energy Transfer Mechanism of Ce^{3+}/Yb^{3+} Codoped Calcium Scandate Phosphor

Jing Li,[†] Li Chen,*[,†] Zhendong Hao,[‡] Xia Zhang,[‡] Ligong Zhang,[‡] Yongshi Luo,[‡] and Jiahua Zhang*[,‡]

[†]School of Basic Sciences, ChangChun University of Technology, A1018 Huguang Road, Changchun 130012, China

[‡]State Key Laboratory of Luminescence and Applications, Changchun Institute of Optics, Fine Mechanics and Physics, Chinese Academy of Sciences, 3888 Eastern South Lake Road, Changchun 130033, China

ABSTRACT: An efficient near-infrared (NIR) downconversion has been demonstrated in $CaSc_2O_4$: Ce^{3+}/Yb^{3+} phosphor. Doping concentration optimized $CaSc_2O_4$: 1%Ce^{3+}/5%Yb^{3+} shows stronger NIR emission than doping concentration also optimized typical YAG: 1%Ce^{3+}/5%Yb^{3+} under 470 nm excitation. The NIR emission from 900 to 1100 nm is enhanced by a factor of 2.4. In addition, the main emission peak of Yb^{3+} in the $CaSc_2O_4$ around 976 nm matches better with the optimal spectral response of the c-Si solar cell. The visible and NIR spectra and the decay curves of Ce^{3+}: 5d → 4f emission were used to demonstrate the energy transfer from Ce^{3+} ions to Yb^{3+} ions. The downconversion phenomenon has been observed under the direct excitation of Ce^{3+} ions. On analyzing the dependence of energy transfer rate on Yb^{3+} ion concentration, we reveal that the energy transfer (ET) from Ce^{3+} ions to Yb^{3+} ions in $CaSc_2O_4$ occurs mainly by the single-step ET process. Considering that the luminescence efficiency of $CaSc_2O_4$: Ce^{3+} is comparable to that of commercial phosphor YAG: Ce^{3+}, the estimated maximum energy transfer efficiency reaches 58% in the $CaSc_2O_4$: 1%Ce^{3+}/15% Yb^{3+} sample, indicating that $CaSc_2O_4$: Ce^{3+}/Yb^{3+} sample has the potential in improving the conversion efficiency of c-Si solar cells.

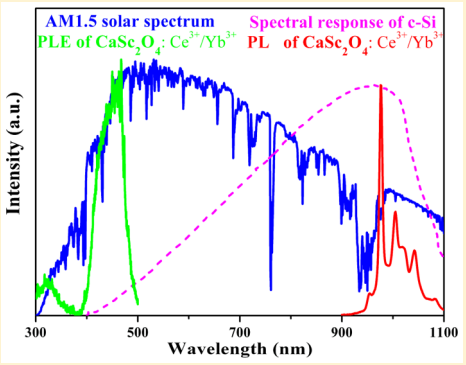

INTRODUCTION

Due to converting sunlight into electricity directly, photovoltaic solar cells are considered as the prime candidates for effective large-scale capture and conversion of the sustainable solar energy.[1,2] At present, the commercial crystalline silicon solar cell (c-Si) dominating the photovoltaic market has an efficiency of only 18%, because the terrestrial spectrum of the solar radiation on the surface of the earth (AM 1.5 G) has a large energy mismatch with the response spectrum of silicon solar cells.[2,3] Silicon solar cells have the strongest absorption around 800−1100 nm.[4] Due to higher reflection and absorption, the response becomes weak in the short wavelength region, especially in the 300−500 nm region.[5] However, the solar spectrum is still very strong in this region.[6] Downconversion (DC) materials have provided a promising way for the enhancement of solar cell efficiency, which can convert the high-energy photons to near-infrared (NIR) photons.[7] Choosing the suitable DC material, the actual efficiency of a silicon solar cell can be improved to about 40%,[7] well over the efficiency limit (29%) estimated by Shockley and Queisser.[8] DC has also been reported in several RE^{3+}/Yb^{3+} couples, such as Pr^{3+}/Yb^{3+}, Tm^{3+}/Yb^{3+}, Tb^{3+}/Yb^{3+}, Er^{3+}/Yb^{3+}, Nd^{3+}/Yb^{3+}, Ho^{3+}/Yb^{3+}, and so on.[9−14] Yb^{3+} ion is suitable as an acceptor and emitter because it has an excited state at approximately 10 000 cm^{-1}, just above the band edge of crystalline silicon.[15] However, the absorption transition of Pr^{3+}, Tb^{3+}, Er^{3+}, Ho^{3+}, and Tm^{3+} as a sensitizer arises from the forbidden 4f → 4f transitions, which are naturally weak in intensity and narrow in bandwidth.[6,16] Unlike these RE ions, the absorption of Ce^{3+} is originated from the allowed 4f → 5d electric-dipole transitions in the broad spectral range, which results in a very high absorption cross section of about 10^{-18} cm^2.[16] The value of the 4f → 4f transitions of RE^{3+} donor ions is merely 10^{-21} cm^2.[16] Moreover, the excitation and emission spectra of Ce^{3+} can be tuned by the host materials, which means that DC from Ce^{3+} to Yb^{3+} can be enhanced by choosing appropriate host materials.[17] The DC of Ce^{3+}/Yb^{3+} combination has been reported in various oxide hosts, such as $Y_3Al_5O_{12}$, borates, silicates, and phosphates.[6,18−21]

$CaSc_2O_4$ as the host lattice which has an orthorhombic $CaFe_2O_4$ structure with space group *Pnam* (No. 62) exhibits low crystal field symmetry and strong crystal field intensity.[22] Low-symmetry hosts exert a crystal field containing more uneven components around the dopant ions which can improve the transition probabilities. The strong crystal field can lead to the large Stark splitting of the energy level of dopant ions, which can improve the energy transfer efficiency. Furthermore, $CaSc_2O_4$ has a low cutoff phonon frequency of 540 cm^{-1}. The low cutoff phonon frequency can inhibit the nonradiative multiphonon relaxation in the DC process.[22] It has been reported as a promising host for achieving efficient DC

Received: February 4, 2015
Published: May 6, 2015

DOI: 10.1021/acs.inorgchem.5b00280
Inorg. Chem. 2015, 54, 4806−4810

luminescence in some DC materials such as the green-emitting $CaSc_2O_4$: Ce^{3+} and $CaSc_2O_4$: Tb^{3+} and red-emitting $CaSc_2O_4$: Eu^{3+}.[23−25] $CaSc_2O_4$ host is proper for doped Ce^{3+} ions, in which the energy of the 4f → 5d electric-dipole transitions for Ce^{3+} locates in the visible region. Besides, the absorption region also matches well with the high-energy part of the solar spectrum, where the solar cells conversion efficiency is very low. In particular, for $CaSc_2O_4$: Ce^{3+} phosphor, its intense green emission under blue light excitation is comparable to the commercial $Y_3Al_5O_{12}$ (YAG): Ce^{3+} phosphor.[23] The Ce^{3+}/Yb^{3+} codoped YAG material as an efficient conversion material for solar cell applications has been studied recently.[6,18] To our knowledge, the DC properties of Ce^{3+}/Yb^{3+} in $CaSc_2O_4$ have not been demonstrated yet.

In the current work, we report the efficient NIR DC in doping concentration optimized $CaSc_2O_4$: 1%Ce^{3+}/5%Yb^{3+} sample, and the NIR emission from 900 to 1100 nm is enhanced by a factor of 2.4, in comparison with that in doping concentration also optimized typical phosphor YAG: 1%Ce^{3+}/5%Yb^{3+}. We study the effect of Yb^{3+} concentration on emission spectra, decay lifetime, energy transfer efficiency, and energy transfer mechanism in $CaSc_2O_4$: Ce^{3+}/Yb^{3+} sample. Results show $CaSc_2O_4$: Ce^{3+}/Yb^{3+} phosphor is a proper material for application in solar cells.

EXPERIMENTAL SECTION

Sample Preparation. The $CaSc_2O_4$: 1%Ce^{3+}/x%Yb^{3+} powder samples were synthesized by a solid state reaction.[25] The constituent oxides or carbonates $CaCO_3$, Sc_2O_3, Yb_2O_3, and CeO_2 were employed as raw materials, which were mixed homogeneously by an agate mortar for 30 min and placed in a crucible with a lid. The crucible was buried by carbon sticks and sintered at 1500 °C for 4 h in CO-reducing atmosphere.

For comparison, in parallel, the YAG: 1%Ce^{3+}/x%Yb^{3+} powder samples were also prepared by the conventional solid state reaction method. Y_2O_3, Al_2O_3, Yb_2O_3, and CeO_2 were mixed in a ratio molar of $(Y_{1-1\%-x\%}Ce_{1\%}Yb_{x\%})_3Al_5O_{12}$. After a good mixing in an agate mortar, the mixture was sintered at 1600 °C for 5 h under a CO reducing atmosphere. Both $CaSc_2O_4$ and YAG samples produced exhibit high crystallinity as evidenced by XRD data. The two powder samples $CaSc_2O_4$: 1%Ce^{3+}/5%Yb^{3+} and YAG: 1%Ce^{3+}/5%Yb^{3+} have been optimized to obtain the highest NIR emission intensity of Yb^{3+} in each host. It turns out that the optimal fractional concentrations of the dopants in the two hosts are the same.

Measurements and Characterization. Powder X-ray diffraction (XRD) data was collected using Cu Kα radiation (λ = 1.54056 Å) on a Bruker D8 advance diffractometer. The excitation and emission spectra were measured using a FLS920 spectrometer (Edinburgh Instruments, U.K.). The fluorescence decay curves of Ce^{3+} were measured by a FL920 fluorescence lifetime spectrometer (Edinburgh Instruments Ltd.). All of the measurements above were performed at room temperature.

RESULTS AND DISCUSSION

The crystal structures characterized by the XRD patterns are shown in Figure 1a for phosphors with nominal compositions of $CaSc_2O_4$: 1%Ce^{3+}/x%Yb^{3+} (x = 0, 5, 15, 30). All experimental XRD patterns of the samples are indexed well to the standard cards of JCPD card 20-0234. $CaSc_2O_4$ has an orthorhombic $CaFe_2O_4$ structure with space group *Pnam* (No. 62) and lattice constants $a \neq b \neq c$, $\alpha = \beta = \gamma = 90°$, as shown in Figure 1b. In this structure, Ca^{2+} is 8-fold with a large effective ionic radius (1.12 Å) and Sc^{3+} 6-fold with a small radius (0.745 Å). The unit cell of $CaSc_2O_4$ shows there is only one site for Ca^{2+} and two coordinated sites for Sc^{3+}. The

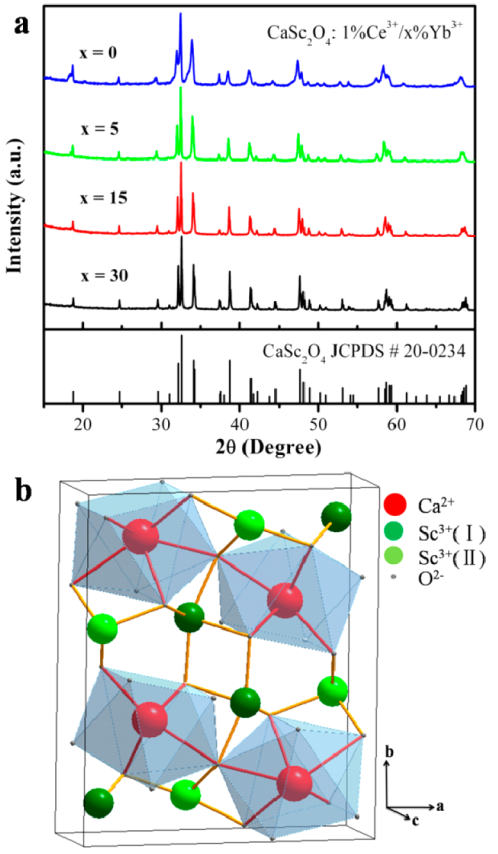

Figure 1. (a) XRD patterns for samples with nominal compositions of $CaSc_2O_4$: 1%Ce^{3+}/x%Yb^{3+} (x = 0, 5, 15, 30). (b) Unit cell of $CaSc_2O_4$.

occupied site of Ce^{3+} is a Ca^{2+} site in the $CaSc_2O_4$; the ionic radius of Ce^{3+} (1.143 Å) is close to that of Ca^{2+}.[23] The Yb^{3+} ions with a large ionic radius (0.868 Å) occupy Sc^{3+} sites in $CaSc_2O_4$, which has been reported in Yb^{3+} singly doped $CaSc_2O_4$ sample.[26] No impurity phase is detected in all XRD patterns, demonstrating that Ce^{3+} and Yb^{3+} substitutions have no effect on the phase structure of $CaSc_2O_4$ host.

In order to investigate the DC properties of Ce^{3+}/Yb^{3+} codoped $CaSc_2O_4$ phosphor, the excitation (PLE) and emission (PL) spectra of samples as direct evidence of Ce^{3+} → Yb^{3+} energy transfer (ET) were measured and are shown in Figures 2 and 3, respectively. In Figure 2, the intense excitation band centered at around 466 nm for monitoring Ce^{3+} emission at

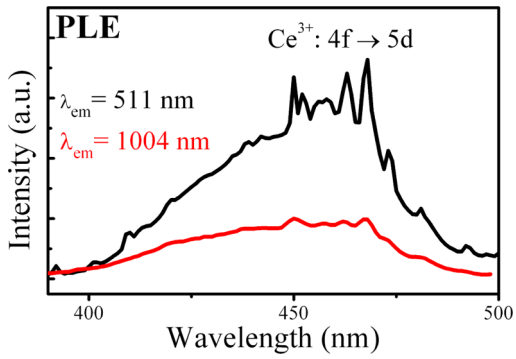

Figure 2. Excitation spectra of Ce^{3+} emission centered at 511 nm (black line) and Yb^{3+} emission at 1004 nm (red line) in $CaSc_2O_4$: 1% $Ce^{3+}/5\%Yb^{3+}$ sample.

DOI: 10.1021/acs.inorgchem.5b00280
Inorg. Chem. 2015, 54, 4806−4810

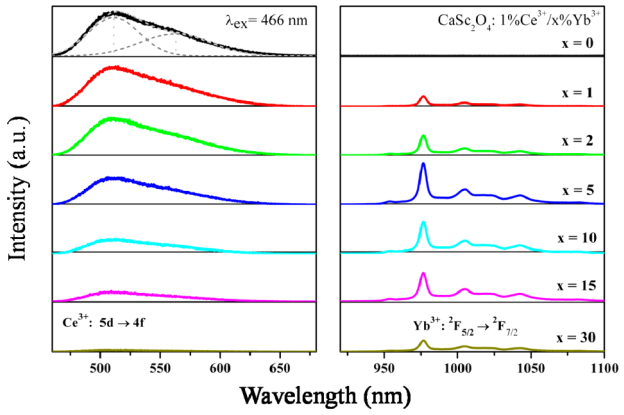

Figure 3. Visible and NIR emission spectra of the samples with nominal compositions of $CaSc_2O_4$: 1%Ce^{3+}/x%Yb^{3+} (x = 0, 1, 2, 5, 10, 15, 30) under 466 nm excitation.

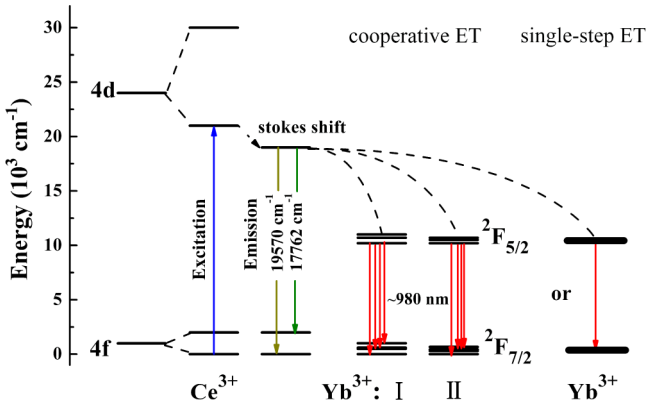

Figure 4. Schematic energy level diagrams of Ce^{3+} and Yb^{3+} with the involved ET process.

511 nm can be assigned to the broad-band absorption of Ce^{3+}: 4f → 5d. The Ce^{3+}: 4f → 5d absorption is also observed by monitoring Yb^{3+} emission at 1004 nm, which indicates the presence of Ce^{3+} → Yb^{3+} ET.

The emission spectra covering the visible and near-infrared spectral range for samples with a fixed Ce^{3+} concentration (1%) and various concentrations of Yb^{3+} are presented under 466 nm excitation corresponding to Ce^{3+}: 4f → 5d absorption in Figure 3. In the visible region (450−700 nm), the broad emission band observed around 511 nm originates from the allowed electronic transition of the excited state 5d to ground state 4f of Ce^{3+} ions. The Ce^{3+} emission can be decomposed into two Gaussian bands centered at about 511 nm (19 570 cm^{-1}) and 563 nm (17 762 cm^{-1}), which are attributed to the transitions from the lowest Stark level of the 5d excited state to different Stark levels ($^2F_{5/2}$ and $^2F_{7/2}$) of the 4f ground state of Ce^{3+}, respectively. The energy difference is about 1808 cm^{-1}, which is very close to the splitting of the 4f ground state of Ce^{3+} ion.[27] In the NIR region (900−1100 nm), a strong emission band around 1000 nm is observed for the Ce^{3+} and Yb^{3+} codoped samples, which is originated from the Yb^{3+}: $^2F_{5/2}$ → $^2F_{7/2}$ transition. The appearance of the NIR emission of Yb^{3+} under direct excitation of Ce^{3+} is another evidence for the existence of ET from Ce^{3+} to Yb^{3+}. It is noticed that the emission intensity of Ce^{3+}: 5d → 4f has a decline with increased Yb^{3+} ion concentration. Simultaneously, the NIR emission of Yb^{3+} first increases and then decreases when the Yb^{3+} concentration exceeds 5% due to concentration quenching.[11] The decreased emission intensity of Ce^{3+} and increased NIR emission intensity of Yb^{3+} when Yb^{3+} concentration increases from 0% to 5% are also proof for the existence of ET from Ce^{3+} to Yb^{3+}. In Ce^{3+}/Yb^{3+} codoped $CaSc_2O_4$ material, x = 5% represents optimal Yb^{3+} doped concentration which is the same as the reported typical phosphor YAG: Ce^{3+}/Yb^{3+}.[6]

The PLE and PL spectra confirm that ET from Ce^{3+} to Yb^{3+} does take place in $CaSc_2O_4$ host lattice. However, more detailed measurements are required in order to understand the energy transfer mechanism clearly. The schematic energy level diagrams with the involved ET process are depicted in Figure 4, in which the proposed energy band diagram of Ce^{3+} is based on the PLE and PL spectra above, and that of Yb^{3+} is from the report of Yb^{3+} singly doped $CaSc_2O_4$ sample by Gaume et al.[26] As shown in the scheme, the ET from the Ce^{3+} to the Yb^{3+} has two possible routes. (1) Cooperative ET, the energy of Ce^{3+} is simultaneously transferred to two nearby Yb^{3+} ions, resulting in two emitting photons of Yb^{3+} with a wavelength around 1000 nm. (2) Single-step ET, it yields only a single NIR photon for each blue photon excitation. It should be noted that a second-order ET is typically 10^3 times less possible than a first-order one, which makes cooperative ET occur with extremely low probability.[28] Recently, Meijerink et al. revealed that a single-step ET instead of a cooperative process took place in the Ce^{3+}/Yb^{3+} codoped YAG material.[6]

For a cooperative ET process, the donor Ce^{3+} transfers its energy simultaneously to two Yb^{3+} ions nearby. For the pair of acceptors, the energy transfer rate (W_{COOP}) is proportional to the square of acceptor concentration. W_{COOP} can be simply written as $W_{COOP} = Cx^2$, where C represents the energy transfer coefficient and x is the Yb^{3+} concentration. For single-step ET process, the Ce^{3+} ion transfers its energy to only one Yb^{3+} ion. Considering that the energy transfer rate (W_{S-S}) is proportional to the acceptor concentration, it can be taken as $W_{S-S} = C'x$.

To judge the process of the ET from Ce^{3+} ions to Yb^{3+} ions in $CaSc_2O_4$ sample, we analyzed the dependence of the energy transfer rate upon Yb^{3+} ion concentration. Figure 5 shows the decay curves of Ce^{3+}: 5d → 4f emission at 511 nm in $CaSc_2O_4$: 1%Ce^{3+}/x%Yb^{3+} (x = 0, 1, 2, 5, 10, 15) under 466 nm

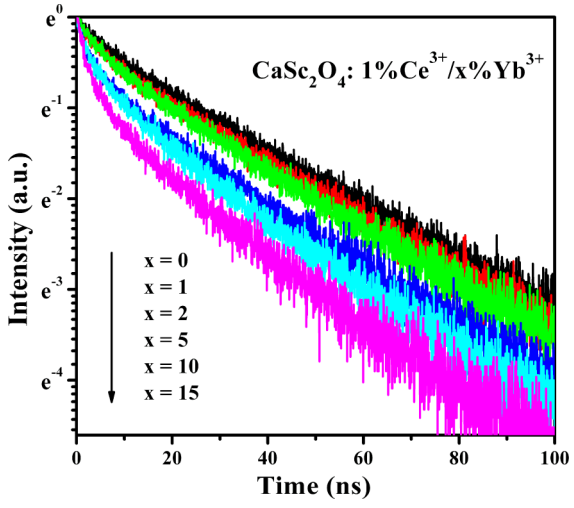

Figure 5. Decay curves of Ce^{3+}: 5d → 4f emission under 466 nm excitation in $CaSc_2O_4$: 1%Ce^{3+}/x%Yb^{3+} (x = 0, 1, 2, 5, 10, 15).

DOI: 10.1021/acs.inorgchem.5b00280
Inorg. Chem. 2015, 54, 4806−4810

excitation. As Yb^{3+} concentration increases, the decays rapidly speed up confirming remarkable $Ce^{3+} \rightarrow Yb^{3+}$ ET. The lifetimes τ_0 and τ of Ce^{3+} in Ce^{3+} singly and Ce^{3+}/Yb^{3+} doubly doped samples are calculated by integrating the area under the corresponding decay curves with the normalized initial intensity. The lifetime values are shown in Table 1. The energy transfer rate (W_{Ce-Yb}) can be obtained by

Table 1. Relationship of Ce^{3+} Lifetime and Energy Transfer Efficiency (η_{ETE}) with Different Concentrations of Yb^{3+} Ions

Yb^{3+} concentrations (%)	τ (ns)	η_{ETE} (%)
0	27.09	0
1	24.02	11
2	22.82	16
5	16.68	38
10	14.89	45
15	11.36	58

$$W_{Ce-Yb} = \frac{1}{\tau} - \frac{1}{\tau_0} \quad (1)$$

In this way, we obtained the Yb^{3+} ion concentration dependence of the energy transfer rates and plotted in a double-logarithmic diagram, as shown in Figure 6. When the concentration of Yb^{3+} ions increases from 1% to 15%, the slope is found to be around 1, indicating the ET from Ce^{3+} ions to Yb^{3+} ions is dominated by the single-step ET process rather than a cooperative ET process. On the basis of above data and analysis, we propose that its probability is low for $Ce^{3+} \rightarrow Yb^{3+}$ ET to get a one-to-two photon process of DC in $CaSc_2O_4$ material.

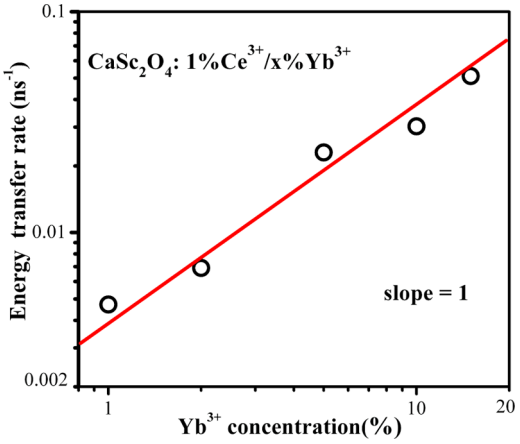

Figure 6. Plot (log–log) of the energy transfer rate versus the Yb^{3+} concentration in $CaSc_2O_4$: $1\%Ce^{3+}/x\%Yb^{3+}$ (x = 0, 1, 2, 5, 10, 15).

With Yb^{3+} concentration increasing, Ce^{3+} lifetime gradually decreases due to the ET from Ce^{3+} to Yb^{3+}, as shown in Figure 5. The variable distribution of Yb^{3+} ions around the Ce^{3+} ions leads to the variety of energy transfer rates; thus, all decay curves exhibit nonexponential characteristics. The energy transfer efficiency (η_{ETE}) can be determined from decay curves. The η_{ETE} is defined as the ratio of Ce^{3+} depopulated by ET to Yb^{3+} over the total number of Ce^{3+} excited. By dividing the integrated intensity of the decay curve of Ce^{3+}/Yb^{3+} codoped $CaSc_2O_4$ sample by that of the Ce^{3+} single doped one, the η_{ETE} is obtained as a function of Yb^{3+} concentration

$$\eta_{ETE,x\%Yb} = 1 - \frac{\tau}{\tau_0} \quad (2)$$

The estimated η_{ETE} of samples presented in Table 1 exhibit a gradual increase with increasing Yb^{3+} concentration. It is worth mentioning that η_{ETE} reaches 58% for $CaSc_2O_4$: $1\%Ce^{3+}/15\%Yb^{3+}$ sample.

Figure 7 shows the normalized PLE and PL spectra of the doping concentration optimized $CaSc_2O_4$: $1\%Ce^{3+}/5\%Yb^{3+}$.

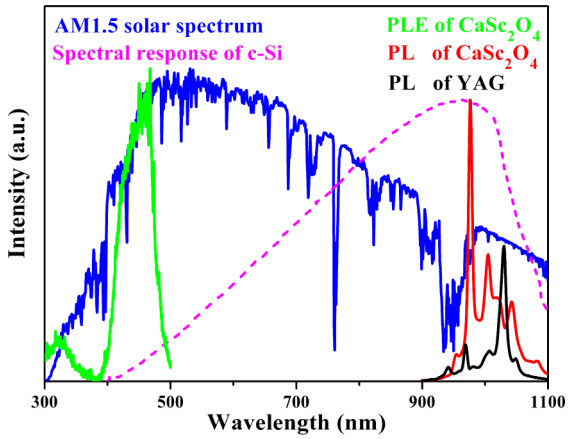

Figure 7. Normalized PLE spectrum of $CaSc_2O_4$: $1\%Ce^{3+}/5\%Yb^{3+}$ (green line), PL spectra of $CaSc_2O_4$: $1\%Ce^{3+}/5\%Yb^{3+}$ (red line), and YAG: $1\%Ce^{3+}/5\%Yb^{3+}$ (black line) excited at 470 nm with the same power density. AM 1.5 G solar spectrum (blue line) and spectral response of c-Si (purple line) are the background.

The background is the AM 1.5 G solar spectrum and the spectral response of c-Si. As shown in Figure 7, the PLE spectrum of $CaSc_2O_4$: $1\%Ce^{3+}/5\%Yb^{3+}$ consists of a blue PLE band around 466 nm corresponding to the transition from the ground state to the lowest-lying 5d state, which agrees with the maximum photon flux region of the solar spectrum and one ultraviolet (UV) PLE band at 320 nm corresponding to the upper 5d states, respectively. Besides, $CaSc_2O_4$: $1\%Ce^{3+}/5\%Yb^{3+}$ gives an intense NIR emission at around 976 nm, matching well with the optimal spectral response of c-Si solar cells. Comparing with doping concentration also optimized typical phosphor YAG: $1\%Ce^{3+}/5\%Yb^{3+}$, doping concentration optimized $CaSc_2O_4$: $1\%Ce^{3+}/5\%Yb^{3+}$ shows the stronger NIR emission. The NIR emission of $CaSc_2O_4$ sample from 900 to 1100 nm is enhanced by a factor of 2.4 excited at 470 nm with the same power density, which corresponds to the best excitation of Ce^{3+} in YAG: Ce^{3+} sample.[29] Furthermore, the main emission peak of Yb^{3+} in the $CaSc_2O_4$ around 976 nm shows better agreement with the optimal spectral response of c-Si compared with that in YAG around 1028 nm. The NIR emission of Yb^{3+} can be used more effectively in the $CaSc_2O_4$. Therefore, $CaSc_2O_4$ is a promising solar spectral converter for achieving efficient NIR emission for c-Si solar cells.

CONCLUSIONS

In summary, an efficient NIR DC has been demonstrated for the $CaSc_2O_4$: $1\%Ce^{3+}/5\%Yb^{3+}$ sample. Compared with that in doping concentration optimized YAG: $1\%Ce^{3+}/5\%Yb^{3+}$, the NIR emission from 900 to 1100 nm is enhanced by a factor of

DOI: 10.1021/acs.inorgchem.5b00280
Inorg. Chem. 2015, 54, 4806−4810

2.4. The main emission peak of Yb^{3+} in the $CaSc_2O_4$ around 976 nm matches well with the optimal spectral response of the c-Si solar cell. Furthermore, the mechanism of the DC process in $CaSc_2O_4$: Ce^{3+}/Yb^{3+} samples has been investigated carefully. On the basis of the analysis of the dependence of the energy transfer rate on Yb^{3+} ion concentration, we propose that the ET from Ce^{3+} ions to Yb^{3+} ions occurs mainly by the single-step ET process. The estimated maximum energy transfer efficiency (η_{ETE}) reaches 58% in the $CaSc_2O_4$: $1\%Ce^{3+}/15\%Yb^{3+}$ sample. The current experimental results indicate that $CaSc_2O_4$: Ce^{3+}/Yb^{3+} sample is a promising DC material for application in solar cells.

AUTHOR INFORMATION

Corresponding Authors

*Phone: +86-431-8571-7353. E-mail: chenli@ccut.edu.cn.

*Phone: +86-431-8617-6317. Fax: +86-431-8617-6317. E-mail: zhangjh@ciomp.ac.cn.

Notes

The authors declare no competing financial interest.

ACKNOWLEDGMENTS

This work was supported by the National Natural Science Foundation of China (11474035, 51172226, 61275055, 11274007) and the Natural Science Foundation of Jilin province (201205024).

REFERENCES

(1) Morton, O. *Nature* **2006**, *443*, 19−22.

(2) M. van der Ende, B.; Aarts, L.; Meijerink, A. *Adv. Mater.* **2009**, *21*, 3073−3077.

(3) Yu, K. H.; Chen, J. H. *Nanoscale Res. Lett.* **2008**, *4*, 1−10.

(4) Richards, B. S. *Sol. Energy Mater. Sol. Cells* **2006**, *90*, 2329−2337.

(5) Strümpel, C.; McCann, M.; Beaucarne, G.; Arkhipov, V.; Slaoui, A.; Švrček, V.; del Cañizo, C.; Tobias, I. *Sol. Energy Mater. Sol. Cells* **2007**, *91*, 238−249.

(6) Yu, D. C.; Rabouw, F. T.; Boon, W. Q.; Kieboom, T.; Ye, S.; Zhang, Q. Y.; Meijerink, A. *Phys. Rev. B* **2014**, *90*, 165126.

(7) Trupke, T.; Green, M. A.; Würfel, P. *J. Appl. Phys.* **2002**, *92*, 1668−1674.

(8) Shockley, W.; Queisser, H. J. *J. Appl. Phys.* **1961**, *32*, 510.

(9) Xiang, G. T.; Zhang, J. H.; Hao, Z. D.; Zhang, X.; Pan, G. H.; Luo, Y. S.; Lü, S. Z.; Zhao, H. F. *Phys. Chem. Chem. Phys.* **2014**, *16*, 9289.

(10) Li, J.; Zhang, J. H.; Zhang, X.; Hao, Z. D.; Luo, Y. S. *J. Alloys Compd.* **2014**, *583*, 96−99.

(11) Vergeer, P.; Vlugt, T.; Kox, M.; den Hertog, M.; van der Eerden, J.; Meijerink, A. *Phys. Rev. B* **2005**, *71*, 014119.

(12) Fan, B.; Chlique, C.; Merdrignac-Conanec, O.; Zhang, X. H.; Fan, X. P. *J. Phys. Chem. C* **2012**, *116*, 11652−11657.

(13) Chen, D.; Yu, Y.; Lin, H.; Huang, P.; Shan, Z.; Wang, Y. *Opt. Lett.* **2010**, *35*, 220−222.

(14) Yu, D. C.; Huang, X. Y.; Ye, S.; Zhang, Q. Y. *J. Alloys Compd.* **2011**, *509*, 9919−9923.

(15) Zhang, J. H.; Hao, Z. D.; Li, J.; Zhang, X.; Luo, Y. S.; Pan, G. H. *Light: Sci. Appl.* **2015**, *4*, e239.

(16) Chen, D. Q.; Wang, Y. S.; Yu, Y. L.; Huang, P.; Weng, F. Y. *J. Appl. Phys.* **2008**, *104*, 116105.

(17) Liu, Z.; Li, J.; Yang, L.; Chen, Q.; Chu, Y.; Dai, N. *Sol. Energy Mater. Sol. Cells* **2014**, *122*, 46−50.

(18) Fang, Z.; Cao, R.; Zhang, F.; Ma, Z.; Dong, G.; Qiu, J. *J. Mater. Chem. C* **2014**, *2*, 2204.

(19) Chen, J.; Zhang, H.; Li, F.; Guo, H. *Mater. Chem. Phys.* **2011**, *128*, 191−194.

(20) Li, Y.; Wang, J.; Zhou, W.; Zhang, G.; Chen, Y.; Su, Q. *Appl. Phys. Express* **2013**, *6*, 082301.

(21) Zhao, L.; Han, L. L.; Wang, Y. H. *Opt. Mater. Express* **2014**, *4*, 1456−1464.

(22) Li, J.; Zhang, J. H.; Hao, Z. D.; Zhang, X.; Zhao, J. H.; Luo, Y. S. *Appl. Phys. Lett.* **2012**, *101*, 121905.

(23) Shimomura, Y.; Kurushima, T.; Kijima, N. *J. Electrochem. Soc.* **2007**, *154*, J234−J238.

(24) Hao, Z. D.; Zhang, J. H.; Zhang, X.; Lü, S. Z.; Wang, X. J. *J. Electrochem. Soc.* **2009**, *156*, H193−H196.

(25) Hao, Z. D.; Zhang, J. H.; Zhang, X.; Wang, X. J. *Opt. Mater.* **2011**, *33*, 355−358.

(26) Gaume, R.; Viana, B.; Derouet, J.; Vivien, D. *Opt. Mater.* **2003**, *22*, 107−115.

(27) Liu, Y. F.; Zhang, X.; Hao, Z. D.; Lü, W.; Liu, X. Y.; Wang, X. J.; Zhang, J. H. *J. Phys. D: Appl. Phys.* **2011**, *44*, 075402.

(28) Blass, G.; Grabmaier, B. C. *Luminescence Materials*; Springer-Verlag, Berlin, 1994.

(29) Wang, L.; Zhang, X.; Hao, Z. D.; Luo, Y. S.; Zhang, J. H.; Wang, X. J. *J. Appl. Phys.* **2010**, *108*, 1.

DOI: 10.1021/acs.inorgchem.5b00280
Inorg. Chem. 2015, 54, 4806−4810